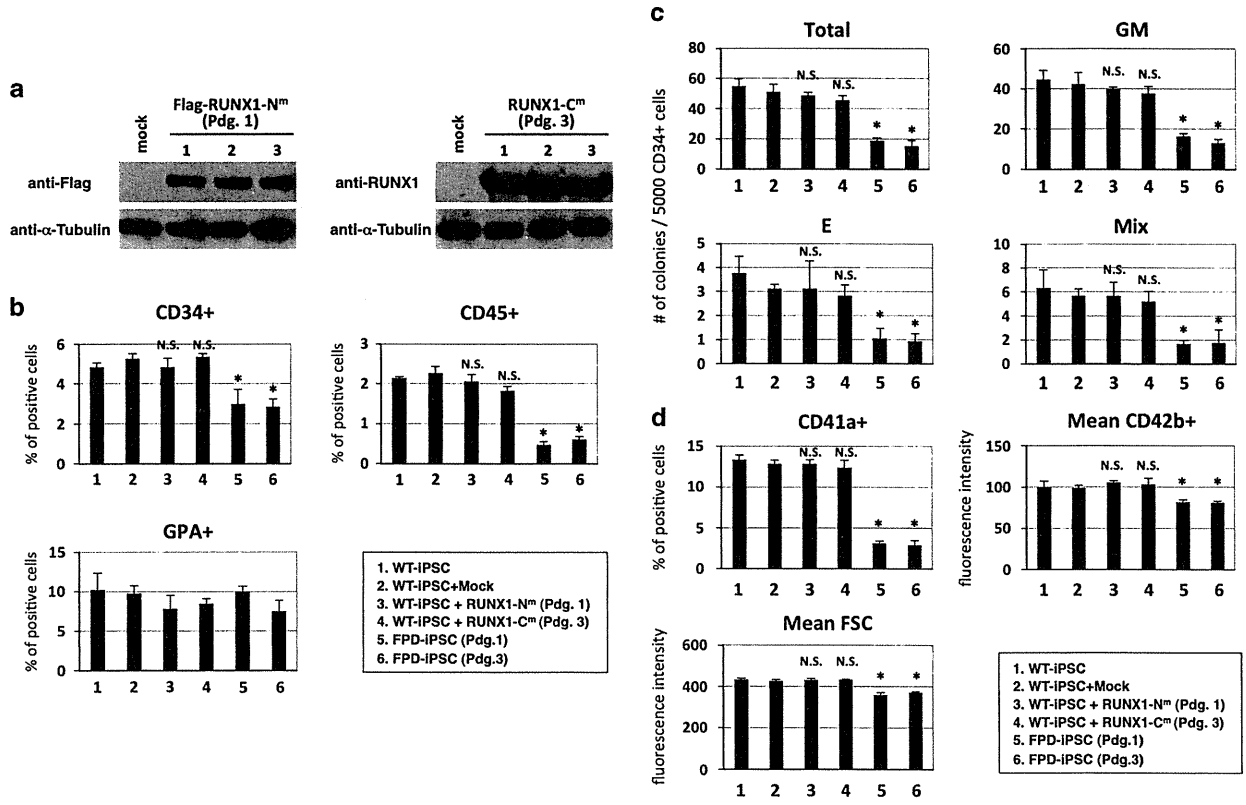

Figure 8. Effects of mutant *RUNX1* on hematopoietic differentiation of WT-iPSCs. (**a**) Expression of mutant RUNX1 protein in WT-iPSCs transfected with pcDNA3/Flag-*RUNX1*-N^m or pcDNA3/*RUNX1*-C^m. Three different clones were isolated for each *RUNX1*-mutant, and the expression of transfected genes was examined by western blotting. Flag-RUNX1-N^m and RUNX1-C^m proteins were detected by anti-Flag and anti-RUNX1 antibodies, respectively. α-Tubulin was used as a loading control. The clone numbers are shown on each lane. WT-iPSCs transfected with mock vector (mock) were used as a negative control. (**b**) Hematopoietic differentiation of WT-iPSCs expressing *RUNX1*-N^m and *RUNX1*-C^m by AGM-S3 co-culture. Cells were co-cultured on AGM-S3 cells for 10–14 days and subjected to FACS analyses. Frequencies (%) of $CD34^+$, $CD45^+$ or GPA^+ cells derived from WT-iPSCs expressing *RUNX1*-N^m and *RUNX1*-C^m or FPD-iPSCs (Pdg. 1 and 3) against MNCs are shown ($n = 3$, mean ± s.d.). Parental WT-iPSCs and WT-iPSCs transfected with mock vector were used as controls. $^*P < 0.05$. NS, not significant against 'WT-iPSCs' or 'WT-iPSCs + mock'. (**c**) Colony-forming assay of HPCs derived from WT-iPSCs expressing *RUNX1*-N^m and *RUNX1*-C^m. Sorted $CD34^+$ cells (5000 cells/plate) from AGM-S3 co-culture were subjected to the assay as described in Methods. GM, CFU-GM; E, BFU-E; Mix, CFU-mix. Data are mean ± s.d. ($n = 3$). $^*P < 0.05$. NS, not significant against 'WT-iPSCs' or 'WT-iPSCs + mock'. Description of the columns is the same as that in panel (**b**) or (**d**). (**d**) Differentiation of MgKs from $CD34^+$ cells derived from WT-iPSCs expressing *RUNX1*-N^m and *RUNX1*-C^m. Percentage of $CD41a^+$ cells, mean fluorescence intensity of CD42b and mean-FSC are shown. Data are mean ± s.d. ($n = 3$). $^*P < 0.05$. NS, not significant against 'WT-iPSCs' or 'WT-iPSCs + mock'.

are defective in DNA binding, dimerization with CBFβ or transactivation capacities,[3,9] and thereby suppress WT-*RUNX1* by varying degrees when they are overexpressed *in vitro*.[3] Taken together, it is plausible that the effects of mutant *RUNX1* on hematopoiesis significantly vary depending on the expression levels and the cellular context. This notion is supported by the previous observation that retroviral overexpression of mutant *Runx1* in BM cells leads to the development of MDS/AML in mice, while heterozygous mutant *Runx1*-KI mice do not develop leukemia during their lifetime. Further investigation is required to reveal precise molecular mechanism for differential effect of *RUNX1* under various conditions.

Ran *et al.*[45] have recently reported that enforced expression of *RUNX1a*, a naturally occurring isoform lacking C-terminal activation/repression domain, enhanced the production of $CD34^+CD45^+$ HPCs from human ESCs/iPSCs, which are transplantable to immune-deficient mice. However, in our hands, overexpression of *RUNX1*^{N233fsX283} mutant (*RUNX1*-C^m), which closely resembles *RUNX1a*, in WT-iPSCs did not affect the differentiation to $CD34^+$ cells. This discrepancy could be due to a slight difference between the sequences of *RUNX1a* and *RUNX1*-C^m, the different strategies taken to deliver *RUNX1* mutants into iPSCs (lentiviral transduction vs plasmid overexpression), integration sites of the transduced gene or different iPSC clones utilized. This is certainly another issue of future investigation.

Another critical finding of this study is a cell-autonomous effect of *RUNX1* mutation on hematopoiesis. Although previous studies using mutant mice or patient samples suggested cell-autonomous effects of mutant *RUNX1* on HPC emergence and MgK differentiation, it has still been possible that extrinsic factors such as altered microenvironmental cues affected the differentiation process *in vivo*. This study demonstrated that FPD-iPSCs were defective in hematopoietic differentiation in *in vitro* assays, showing that disease-specific *RUNX1* mutation impaired the emergence of HPCs and MgK differentiation indeed in a cell-autonomous manner.

It is noteworthy that functional roles of mutant *RUNX1* on MgK differentiation and platelet production are critically different between humans and mice. In mice, heterozygous DNA-binding *Runx1* mutation never led to thrombocytopenia, and only homozygous animals presented mild MgK/platelet defects.[9] In contrast, heterozygous *RUNX1* mutation is sufficient to cause MgK defects in human settings as demonstrated by the current study. These differences could be due to a differential sensitivity of MgK

differentiation and platelet production to *RUNX1* dosage in human or mouse hematopoiesis. Molecular mechanism underlying this discrepancy definitely requires further investigation.

In MgK differentiation assays, mean-FSC by flow cytometry was significantly lower in MgKs derived from FPD-iPSCs as compared with those from WT-iPSCs, suggesting that FPD-iPSC-derived MgKs are smaller in size. Complementation of *RUNX1* activity in FPD-iPSCs by WT-*RUNX1* rescued MgK differentiation as examined by CD41a expression. Interestingly, however, mean-FSC of FPD-iPSC-derived MgKs did not return to the level comparable to that of WT in the same experiment. These results indicated that differentiation and cell size of MgKs were differentially regulated by *RUNX1* and raise a possibility that reduced size of FPD-iPSC-derived MgKs might be the consequence of novel function acquired by mutant *RUNX1*.

We were able to analyze three FPD-iPSC lines derived from three distinct FPD/AML pedigrees. Two pedigrees carried mutation in RUNT domain that disrupts DNA binding, and the other carried frame-shift mutation resulting in premature termination before C-terminal activation/repression domain. Through our *in vitro* hematopoietic differentiation analyses, we could find no major difference between the three FPD-iPSC lines in terms of HPC emergence and MgK differentiation. These results suggest that disease-specific *RUNX1* mutations impose highly similar impact on the hematopoietic differentiation of iPSCs regardless of the sites of mutation. However, it still leaves a possibility that various *RUNX1* mutations differentially affect other aspects of hematopoiesis. Particularly, as mutant *RUNX1* is involved in the malignant transformation of hematopoietic cells, it would be intriguing to examine differential impacts of various *RUNX1* mutations on the development of AML or MDS using our FPD-iPSC models.

In summary, we have successfully established iPSCs from three distinct FPD/AML pedigrees and have shown that these FPD-iPSCs are uniformly defective in HPC emergence and MgK differentiation. This report is the first to demonstrate critical roles of *RUNX1* in hematopoiesis in human experimental settings and revealed differential impact of heterozygous mutant *RUNX1* on human and mouse MgK differentiation. We also demonstrated that the phenotypes of FPD-iPSCs are the consequence of haploinsufficiency of *RUNX1*. We expect that these FPD-iPSC lines are extremely useful as an unlimited source for human HPCs with various *RUNX1* mutations, and they will serve as a novel platform for investigating multistep leukemogenesis based on *RUNX1* mutation.

CONFLICT OF INTEREST

HO is the scientific consultant of San Bio, Inc., Eisai Co Ltd. and Daiichi Sankyo Co Ltd. HN is a founder, a member of scientific advisory board and shareholder of ReproCELL and is a scientific advisor of Megakaryon, iCELL and Shionogi & Co. The remaining authors declare no conflict of interest.

ACKNOWLEDGEMENTS

We thank excellent technical assistance by J Kawakita. We also thank S Suzuki (FACS Core Laboratory, Keio University School of Medicine) for FACS sorting, W Akamatsu and M Sato (Department of Physiology, Keio University School of Medicine) and H Nakata (Division of Cardiology, Keio University School of Medicine) for cell culture or establishment of iPSCs. This work was supported in part by a grant from the Ministry of Education, Culture, Sports, Science and Technology of Japan.

REFERENCES

1 Ichikawa M, Asai T, Saito T, Seo S, Yamazaki I, Yamagata T *et al.* AML-1 is required for megakaryocytic maturation and lymphocytic differentiation, but not for maintenance of hematopoietic stem cells in adult hematopoiesis. *Nat Med* 2004; **10**: 299–304.
2 Osato M. Point mutations in the RUNX1/AML1 gene: another actor in RUNX leukemia. *Oncogene* 2004; **23**: 4284–4296.
3 Harada H, Harada Y, Niimi H, Kyo T, Kimura A, Inaba T. High incidence of somatic mutations in the AML1/RUNX1 gene in myelodysplastic syndrome and low blast percentage myeloid leukemia with myelodysplasia. *Blood* 2004; **103**: 2316–2324.
4 Christiansen DH, Andersen MK, Pedersen-Bjergaard J. Mutations of AML1 are common in therapy-related myelodysplasia following therapy with alkylating agents and are significantly associated with deletion or loss of chromosome arm 7q and with subsequent leukemic transformation. *Blood* 2004; **104**: 1474–1481.
5 Harada H, Harada Y, Tanaka H, Kimura A, Inaba T. Implications of somatic mutations in the AML1 gene in radiation-associated and therapy-related myelodysplastic syndrome/acute myeloid leukemia. *Blood* 2003; **101**: 673–680.
6 Zharlyganova D, Harada H, Harada Y, Shinkarev S, Zhumadilov Z, Zhunusova A *et al.* High frequency of AML1/RUNX1 point mutations in radiation-associated myelodysplastic syndrome around Semipalatinsk nuclear test site. *J Radiat Res* 2008; **49**: 549–555.
7 Kuo MC, Liang DC, Huang CF, Shih YS, Wu JH, Lin TL *et al.* RUNX1 mutations are frequent in chronic myelomonocytic leukemia and mutations at the C-terminal region might predict acute myeloid leukemia transformation. *Leukemia* 2009; **23**: 1426–1431.
8 Ernst T, Chase A, Zoi K, Waghorn K, Hidalgo-Curtis C, Score J *et al.* Transcription factor mutations in myelodysplastic/myeloproliferative neoplasms. *Haematologica* 2010; **95**: 1473–1480.
9 Matheny CJ, Speck ME, Cushing PR, Zhou Y, Corpora T, Regan M *et al.* Disease mutations in RUNX1 and RUNX2 create nonfunctional, dominant-negative, or hypomorphic alleles. *EMBO J* 2007; **26**: 1163–1175.
10 Harada Y, Harada H. Molecular pathways mediating MDS/AML with focus on AML1/RUNX1 point mutations. *J Cell Physiol* 2009; **220**: 16–20.
11 Michaud J, Wu F, Osato M, Cottles GM, Yanagida M, Asou N *et al.* In vitro analyses of known and novel RUNX1/AML1 mutations in dominant familial platelet disorder with predisposition to acute myelogenous leukemia: implications for mechanisms of pathogenesis. *Blood* 2002; **99**: 1364–1372.
12 Imai Y, Kurokawa M, Izutsu K, Hangaishi A, Takeuchi K, Maki K *et al.* Mutations of the AML1 gene in myelodysplastic syndrome and their functional implications in leukemogenesis. *Blood* 2000; **96**: 3154–3160.
13 Song WJ, Sullivan MG, Legare RD, Hutchings S, Tan X, Kufrin D *et al.* Haploinsufficiency of CBFA2 causes familial thrombocytopenia with propensity to develop acute myelogenous leukaemia. *Nat Genet* 1999; **23**: 166–175.
14 Higuchi M, O'Brien D, Kumaravelu P, Lenny N, Yeoh EJ, Downing JR. Expression of a conditional AML1-ETO oncogene bypasses embryonic lethality and establishes a murine model of human t(8;21) acute myeloid leukemia. *Cancer Cell* 2002; **1**: 63–74.
15 Motoda L, Osato M, Yamashita N, Jacob B, Chen LQ, Yanagida M *et al.* Runx1 protects hematopoietic stem/progenitor cells from oncogenic insult. *Stem Cells* 2007; **25**: 2976–2986.
16 Jacob B, Osato M, Yamashita N, Wang CQ, Taniuchi I, Littman DR *et al.* Stem cell exhaustion due to Runx1 deficiency is prevented by Evi5 activation in leukemogenesis. *Blood* 2010; **115**: 1610–1620.
17 Takahashi K, Tanabe K, Ohnuki M, Narita M, Ichisaka T, Tomoda K *et al.* Induction of pluripotent stem cells from adult human fibroblasts by defined factors. *Cell* 2007; **131**: 861–872.
18 Yu J, Vodyanik MA, Smuga-Otto K, Antosiewicz-Bourget J, Frane JL, Tian S *et al.* Induced pluripotent stem cell lines derived from human somatic cells. *Science* 2007; **318**: 1917–1920.
19 Chou ST, Byrska-Bishop M, Tober JM, Yao Y, Vandorn D, Opalinska JB *et al.* Trisomy 21-associated defects in human primitive hematopoiesis revealed through induced pluripotent stem cells. *Proc Natl Acad Sci USA* 2012; **109**: 17573–17578.
20 Ye Z, Zhan H, Mali P, Dowey S, Williams DM, Jang YY *et al.* Human-induced pluripotent stem cells from blood cells of healthy donors and patients with acquired blood disorders. *Blood* 2009; **114**: 5473–5480.
21 Park IH, Arora N, Huo H, Maherali N, Ahfeldt T, Shimamura A *et al.* Disease-specific induced pluripotent stem cells. *Cell* 2008; **134**: 877–886.
22 Hiramoto T, Ebihara Y, Mizoguchi Y, Nakamura K, Yamaguchi K, Ueno K *et al.* Wnt3a stimulates maturation of impaired neutrophils developed from severe congenital neutropenia patient-derived pluripotent stem cells. *Proc Natl Acad Sci USA* 2013; **110**: 3023–3028.
23 Maclean GA, Menne TF, Guo G, Sanchez DJ, Park IH, Daley GQ *et al.* Altered hematopoiesis in trisomy 21 as revealed through in vitro differentiation of isogenic human pluripotent cells. *Proc Natl Acad Sci USA* 2012; **109**: 17567–17572.
24 Chang CJ, Bouhassira EE. Zinc-finger nuclease-mediated correction of alpha-thalassemia in iPS cells. *Blood* 2012; **120**: 3906–3914.
25 Carette JE, Pruszak J, Varadarajan M, Blomen VA, Gokhale S, Camargo FD *et al.* Generation of iPSCs from cultured human malignant cells. *Blood* 2010; **115**: 4039–4042.

26 Kumano K, Arai S, Hosoi M, Taoka K, Takayama N, Otsu M *et al.* Generation of induced pluripotent stem cells from primary chronic myelogenous leukemia patient samples. *Blood* 2012; **119**: 6234–6242.
27 Gandre-Babbe S, Paluru P, Aribeana C, Chou ST, Bresolin S, Lu L *et al.* Patient-derived induced pluripotent stem cells recapitulate hematopoietic abnormalities of juvenile myelomonocytic leukemia. *Blood* 2013; **121**: 4925–4929.
28 Seki T, Yuasa S, Fukuda K. Generation of induced pluripotent stem cells from a small amount of human peripheral blood using a combination of activated T cells and Sendai virus. *Nat Protoc* 2012; **7**: 718–728.
29 Fukuchi Y, Shibata F, Ito M, Goto-Koshino Y, Sotomaru Y, Ito M *et al.* Comprehensive analysis of myeloid lineage conversion using mice expressing an inducible form of C/EBP alpha. *EMBO J* 2006; **25**: 3398–3410.
30 Ma F, Wang D, Hanada S, Ebihara Y, Kawasaki H, Zaike Y *et al.* Novel method for efficient production of multipotential hematopoietic progenitors from human embryonic stem cells. *Int J Hematol* 2007; **85**: 371–379.
31 Ma F, Ebihara Y, Umeda K, Sakai H, Hanada S, Zhang H *et al.* Generation of functional erythrocytes from human embryonic stem cell-derived definitive hematopoiesis. *Proc Natl Acad Sci USA* 2008; **105**: 13087–13092.
32 Takayama N, Nishikii H, Usui J, Tsukui H, Sawaguchi A, Hiroyama T *et al.* Generation of functional platelets from human embryonic stem cells in vitro via ES-sacs, VEGF-promoted structures that concentrate hematopoietic progenitors. *Blood* 2008; **111**: 5298–5306.
33 Nakajima H, Ito M, Smookler DS, Shibata F, Fukuchi Y, Morikawa Y *et al.* TIMP-3 recruits quiescent hematopoietic stem cells into active cell cycle and expands multipotent progenitor pool. *Blood* 2010; **116**: 4474–4482.
34 Seki T, Yuasa S, Oda M, Egashira T, Yae K, Kusumoto D *et al.* Generation of induced pluripotent stem cells from human terminally differentiated circulating T cells. *Cell Stem Cell* 2010; **7**: 11–14.
35 Xu MJ, Tsuji K, Ueda T, Mukouyama YS, Hara T, Yang FC *et al.* Stimulation of mouse and human primitive hematopoiesis by murine embryonic aorta-gonad-mesonephros-derived stromal cell lines. *Blood* 1998; **92**: 2032–2040.
36 Vodyanik MA, Thomson JA, Slukvin II. Leukosialin (CD43) defines hematopoietic progenitors in human embryonic stem cell differentiation cultures. *Blood* 2006; **108**: 2095–2105.
37 Choi KD, Yu J, Smuga-Otto K, Salvagiotto G, Rehrauer W, Vodyanik M *et al.* Hematopoietic and endothelial differentiation of human induced pluripotent stem cells. *Stem Cells* 2009; **27**: 559–567.
38 Dowdy CR, Xie R, Frederick D, Hussain S, Zaidi SK, Vradii D *et al.* Definitive hematopoiesis requires Runx1 C-terminal-mediated subnuclear targeting and transactivation. *Hum Mol Genet* 2010; **19**: 1048–1057.
39 Okuda T, van Deursen J, Hiebert SW, Grosveld G, Downing JR. AML1 the target of multiple chromosomal translocations in human leukemia, is essential for normal fetal liver hematopoiesis. *Cell* 1996; **84**: 321–330.
40 Wang Q, Stacy T, Binder M, Marin-Padilla M, Sharpe AH, Speck NA. Disruption of the Cbfa2 gene causes necrosis and hemorrhaging in the central nervous system and blocks definitive hematopoiesis. *Proc Natl Acad Sci USA* 1996; **93**: 3444–3449.
41 North T, Gu TL, Stacy T, Wang Q, Howard L, Binder M *et al.* Cbfa2 is required for the formation of intra-aortic hematopoietic clusters. *Development* 1999; **126**: 2563–2575.
42 North TE, de Bruijn MF, Stacy T, Talebian L, Lind E, Robin C *et al.* Runx1 expression marks long-term repopulating hematopoietic stem cells in the midgestation mouse embryo. *Immunity* 2002; **16**: 661–672.
43 Lancrin C, Sroczynska P, Stephenson C, Allen T, Kouskoff V, Lacaud G. The haemangioblast generates haematopoietic cells through a haemogenic endothelium stage. *Nature* 2009; **457**: 892–895.
44 Chen MJ, Yokomizo T, Zeigler BM, Dzierzak E, Speck NA. Runx1 is required for the endothelial to haematopoietic cell transition but not thereafter. *Nature* 2009; **457**: 887–891.
45 Ran D, Shia WJ, Lo MC, Fan JB, Knorr DA, Ferrell PI *et al.* RUNX1a enhances hematopoietic lineage commitment from human embryonic stem cells and inducible pluripotent stem cells. *Blood* 2013; **121**: 2882–2890.

Supplementary Information accompanies this paper on the Leukemia website (http://www.nature.com/leu)

Journal of Molecular and Cellular Cardiology 72 (2014) 241–249

Contents lists available at ScienceDirect

Journal of Molecular and Cellular Cardiology

journal homepage: www.elsevier.com/locate/yjmcc

Original article

Time-lapse imaging of cell cycle dynamics during development in living cardiomyocyte

Hisayuki Hashimoto [a], Shinsuke Yuasa [a,*], Hidenori Tabata [b], Shugo Tohyama [a], Nozomi Hayashiji [a], Fumiyuki Hattori [a], Naoto Muraoka [a], Toru Egashira [a], Shinichiro Okata [a], Kojiro Yae [a], Tomohisa Seki [a], Takahiko Nishiyama [a], Kazunori Nakajima [b], Asako Sakaue-Sawano [c,d], Atsushi Miyawaki [c,d], Keiichi Fukuda [a]

[a] Department of Cardiology, Keio University School of Medicine, Tokyo 160-8582, Japan
[b] Department of Anatomy, Keio University School of Medicine, Tokyo 160-8582, Japan
[c] Life Function and Dynamics, ERATO, JST, 2-1 Hirosawa Wako-city, Saitama 351-0198, Japan
[d] Laboratory for Cell Function and Dynamics, Advanced Technology Development Group, Brain Science Institute, RIKEN, 2-1 Hirosawa, Wako-city, Saitama 351-0198, Japan

ARTICLE INFO

Article history:
Received 3 March 2014
Accepted 24 March 2014
Available online 3 April 2014

Keywords:
Cardiac development
Cell cycle
Imaging
Cardiac regeneration
Cell culture

ABSTRACT

Mammalian cardiomyocytes withdraw from the cell cycle shortly after birth, although it remains unclear how cardiomyocyte cell cycles behave during development. Compared to conventional immunohistochemistry in static observation, time-lapse imaging can reveal comprehensive data in hard-to-understand biological phenomenon. However, there are no reports of an established protocol of successful time-lapse imaging in mammalian heart. Thus, it is valuable to establish a time-lapse imaging system to enable the observation of cell cycle dynamics in living murine cardiomyocytes. This study sought to establish time-lapse imaging of murine heart to study cardiomyocyte cell cycle behavior. The Fucci (fluorescent ubiquitination-based cell cycle indicator) system can effectively label individual G1, S/G2/M, and G1/S-transition phase nuclei red, green and yellow, respectively, in living mammalian cells, and could therefore be useful to visualize the real-time cell cycle transitions in living murine heart. To establish a similar system for time-lapse imaging of murine heart, we first developed an ex vivo culture system, with the culture conditions determined in terms of sample state, serum concentration, and oxygen concentration. The optimal condition (slice culture, oxygen concentration 20%, serum concentration 10%) successfully mimicked physiological cardiomyocyte proliferation in vivo. Time-lapse imaging of cardiac slices from E11.5, E14.5, E18.5, and P1 Fucci-expressing transgenic mice revealed an elongated S/G2/M phase in cardiomyocytes during development. Our time-lapse imaging of murine heart revealed a gradual elongation of the S/G2/M phase during development in living cardiomyocytes.

1. Introduction

Mammalian *cardiomyocytes withdraw* from the *cell cycle* shortly after birth [1], and adult mammalian heart has a limited regenerative capacity [2,3]. Murine neonates show cardiac regenerative capacity after heart damage, but lose this ability soon after birth [4]. To control cardiomyocyte proliferation for cardiac regenerative therapy, it is important to know how and when mammalian cardiomyocytes lose their proliferative capacity. Previous measurements of cycling cells have relied chiefly on immunostaining for cell cycle markers and nucleotide analogue incorporation, both of which assess the static condition in fixed samples [5]. Thus, little is known about the spatial and temporal patterns of mammalian cardiomyocyte cell cycle dynamics during development [6]. The static observations confirmed that cardiomyocyte proliferation ability drops after birth, but it remains unclear whether the cell cycle stops suddenly during development or if it gradually elongates until stopped.

During cardiac tissue morphogenesis, cell proliferation, differentiation, and movement are tightly regulated spatiotemporally by humoral factors and cell–cell interactions [7]. Since cell dissociation affects this cell–cell interaction, in vitro cell cycle analysis using dissociated cardiomyocytes may not accurately represent spatial dynamic information or the in vivo cell cycle dynamics. Ex vivo culture system and live imaging in brain tissue successfully revealed in vivo phenomena such as neuron migration and asymmetrical cell division [8,9]. Ex vivo cardiac culture system and live imaging, which provide less alteration of natural conditions, would overcome these problems. It was recently reported that interlocking fluorescent probes with antiphase oscillating proteins that mark cell cycle transitions could effectively label individual cell cycle stages in living mammalian cells (G1 phase nuclei red, S/G2/M phase green, and G1/S transition phase yellow) [10]. This novel technique, named Fucci (fluorescent ubiquitination-based cell cycle indicator), could be an ideal tool to evaluate cardiomyocyte cell cycle length by visualizing real-time cell cycle transitions in living murine

* Corresponding author at: Department of Cardiology, Keio University School of Medicine, 35 Shinanomachi Shinjuku-ku, Tokyo 160-8582, Japan. Tel.: +81 3 5363 3373; fax: +81 3 5363 3875.
E-mail address: yuasa@a8.keio.jp (S. Yuasa).

http://dx.doi.org/10.1016/j.yjmcc.2014.03.020
0022-2828/

cardiomyocytes using live imaging, particularly in association with an ex vivo culture method.

In this study we therefore sought to establish an ex vivo cardiac culture method for live imaging and elucidate the native cardiomyocyte cell cycle dynamics. Combining the Fucci system with our ex vivo culture method, we observed cardiomyocyte cell cycle progression and gradual elongation of the S/G2/M phase during development in living cardiomyocytes. This is the first study to report direct measurement of the cardiomyocyte cell cycle phase duration, by establishing a live imaging method of ex vivo cultured cardiac tissue.

2. Methods

2.1. Animals

The Fucci-expressing (FucciG1-#596, FucciS/G2/M-#504) mice were established using the CAG promoter, as described previously [10]. Pregnant and neonatal C57BL/6J wild-type mice were purchased from Japan CLEA. Adult mice were anesthetized by 3% isoflurane gas inhalation. Embryos and neonates were anesthetized by cooling on an ice bed for 3 min. The adequacy of anesthesia was monitored by heart rate, muscle relaxation, and the loss of sensory reflex response, i.e. non-response to tail pinching. All experiments were performed in accordance with the Keio University animal care guidelines and approved by the Ethics Committee of Keio University, which conforms to the Guide for the Care and Use of Laboratory Animals published by the US National Institutes of Health (NIH Publication no. 85-23, revised 1996).

2.2. Statistical analyses

Values are presented as mean ± SEM. Statistical significance was evaluated with Student's unpaired *t* test for comparisons between two mean values. $P < 0.05$ was considered significant.

3. Results

3.1. Fucci visualized the cardiomyocyte cell cycle

The cell cycle is finely controlled by ubiquitin-mediated proteolysis. APC^{Cdh1} and SCF^{Skp2} are ubiquitin ligase complexes which mark a variety of proteins with ubiquitin in a cell cycle-dependent manner [11]. Geminin and Cdt1, which are involved in "licensing" of replication origins, are direct substrates of APC^{Cdh1} and SCF^{Skp2}, respectively [12]. Due to cell cycle-dependent proteolysis, protein levels of Geminin and Cdt1 oscillate inversely. Cdt1 levels are highest during the G1 phase and Geminin levels are highest during the S/G2/M phases. By fusing the ubiquitination domains of Geminin and Cdt1 to fluorescent proteins Azami Green and Kusabira Orange respectively, Fucci probes effectively label individual G1 phase nuclei red, G1/S phase nuclei yellow, and S/G2/M phase nuclei green in HeLa and neural cells [10].

In the present study, we first sought to confirm that Fucci probes could distinguish the cell cycle phase in cardiomyocytes. Hearts were extracted from Fucci-red/green transgenic mice (#596/#504) at E18.5 (E0 = the day of plug), and immunostained for Nkx2.5 to identify cardiomyocytes (Fig. 1A). Nkx2.5-positive cells expressed either Fucci-green or Fucci-red, or both as yellow, in E18.5 embryonic ventricular heart (Fig. 1A, B). To confirm that Fucci probes could adequately visualize cell cycle dynamics in cardiomyocytes, we also immunostained for PCNA and PHH3, known as well-established markers of S phase and M phases, respectively [13,14]. Both PCNA- and PHH3-positive cells also showed Fucci-green (Fig. 1C). On the other hand, Fucci-red(+)/green(−) cells did not show any signal for PCNA or PHH3. These data indicated that murine cardiomyocytes express Fucci probes in a proper fashion that reflects the native cell cycle dynamics.

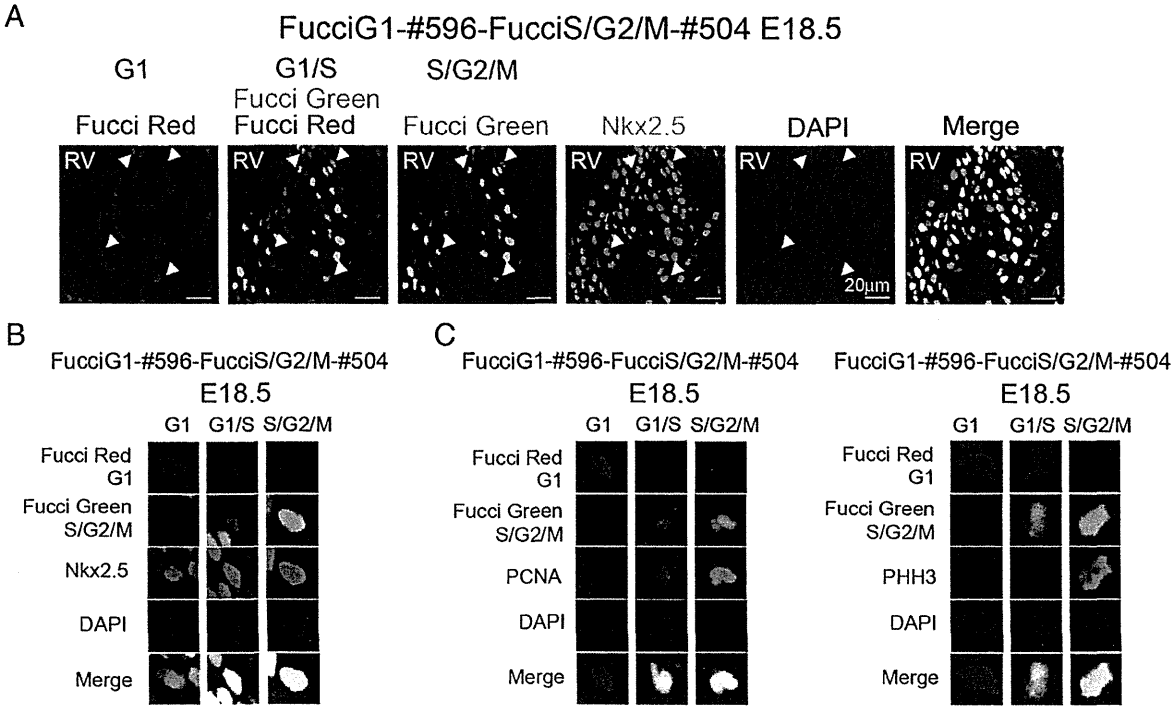

Fig. 1. The cardiomyocyte cell cycle dynamics visualized by Fucci. A. The sections of right ventricles were extracted from Fucci-expressing (#596/#504) mouse embryos at E18.5. Fluorescence images of Fucci green, Fucci red, and cells immunostained for Nkx2.5 and nuclei (DAPI). White arrowheads indicate S/G2/M phase cardiomyocytes. Scale bars, 20 μm. B. Fluorescence images of cardiomyocytes expressing Fucci red and Fucci green and immunofluorescence for Nkx2.5 and DAPI at G1, G1/S and S/G2/M phases. C. Fluorescence images of cardiomyocytes expressing Fucci red and Fucci green and immunofluorescence for PCNA or PHH3, and DAPI at G1, G1/S and S/G2/M phases.

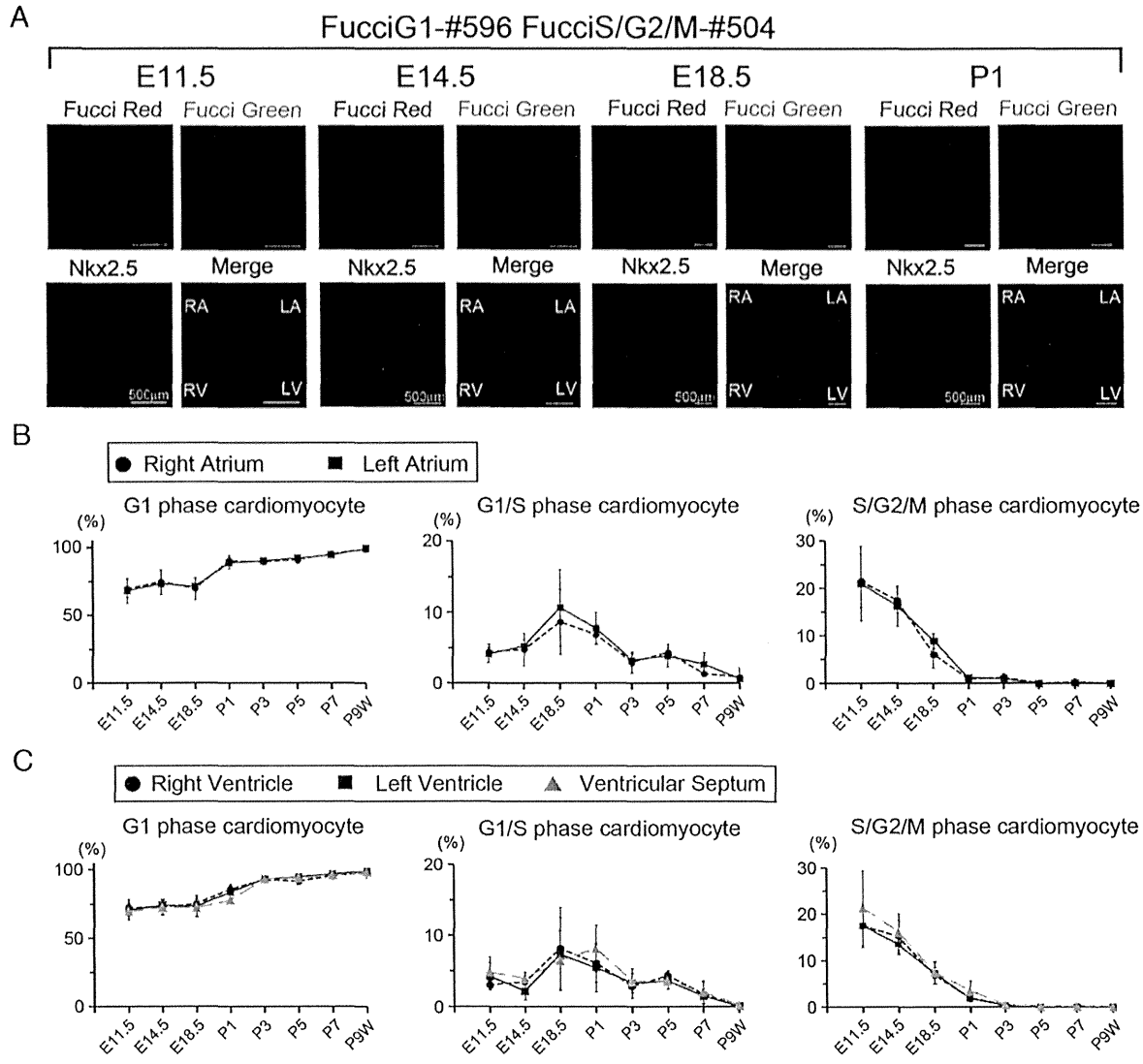

Fig. 2. Cardiomyocyte cell cycle analysis by Fucci probe in the developing heart. A. The sections of heart samples were obtained from Fucci-expressing (#596/#504) mouse embryos from E11.5 to P1. Fluorescence images of cardiomyocytes expressing Fucci green, Fucci red, and cells immunostained for Nkx2.5. Scale bars, 500 μm. B. Percentages of G1, G1/S and S/G2/M phase cardiomyocytes in right atrium and left atrium ($n = 3$–5). C. Percentages of G1, G1/S and S/G2/M phase cardiomyocytes in left ventricle, right ventricle and ventricular septum ($n = 3$–5).

3.2. The Fucci system could visualize developing cardiomyocytes

We next analyzed the cardiomyocyte cell cycle dynamics in Fucci-expressing mouse embryos from E11.5 to P9 weeks. Low-magnification observation revealed the global cell cycle dynamics in developing hearts, with Fucci-green-positive cells gradually decreasing and Fucci-red-positive cells increasing in developing hearts (Fig. 2A). Careful observation revealed that the population of Fucci probe expressing cells has a positive correlation with cardiomyocyte marker expressing cells in the heart (Fig. S1A). Fucci probe expression is under the control of CAG promoter, which could be driven in many cell types [15,16]. We measured the Fucci fluorescence intensity in cardiomyocytes and non-cardiomyocytes, revealing a markedly stronger signal in cardiomyocytes compared to non-cardiomyocytes in the heart (Fig. S1B). For further analysis, heart ventricles from wild-type and Fucci-green-expressing E14.5 mice were compared by FACS (Fig. S1C). The cardiomyocyte proportions detected by cardiac troponin T (cTnT) in both groups were approximately 40%, which is consistent with prior reports [17–19]. The percentage of Fucci-green-positive cardiomyocytes (6.1/38.1 = 16.0%) matched the results from fixed cardiac tissues (Fig. 2C right; E14.5: 18.3%). As expected, the fluorescent intensity of Fucci-green was several orders of magnitude higher in cTnT-positive cells than in cTnT-negative cells. We also assessed the mRNA expression in populations of different Fucci fluorescence intensities. Heart ventricles were extracted from Fucci-red/green-expressing E14.5 mice and cells were sorted into two groups by the strength of Fucci fluorescence intensity. Cardiomyocyte marker expressions such as *Troponin T2* (*Tnnt2*) and *Myosin light chain 2v* (*Myl2*) were extremely stronger in high Fucci fluorescence intensity population compared to low intensity population (Fig. S1D).

3.3. The Fucci system could visualize developing cardiomyocyte cell cycle dynamics

High-magnification imaging revealed similar regional cell cycle dynamics, confirmed by counting the G1, G1/S, and S/G2/M phase cardiomyocytes in the right and left atrium, right and left ventricle, and the interventricular septum. The G1 phase cardiomyocyte population was at a minimum in E11.5 and increased with development. The G1/S phase cardiomyocyte population showed a small peak in E18.5. The S/

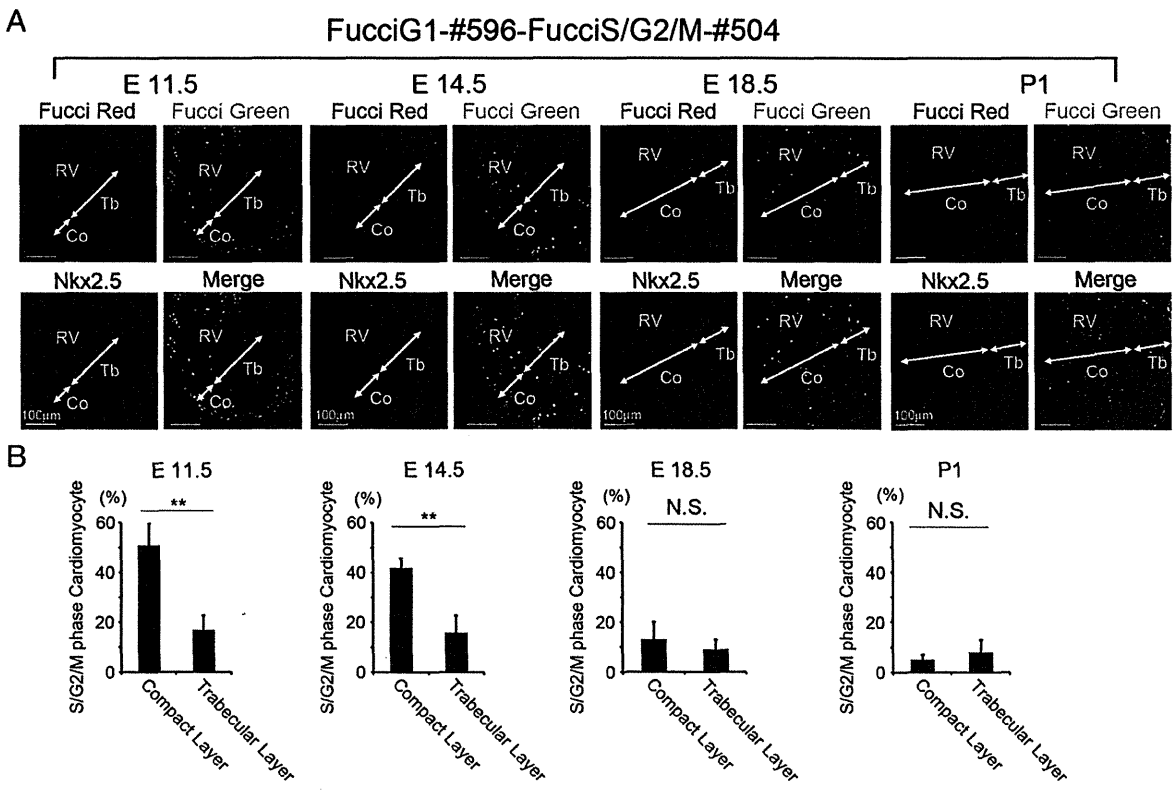

Fig. 3. Regional difference of cell cycle dynamics in the developing cardiac ventricles. A. The sections of right ventricles were obtained from Fucci-expressing (#596/#504) mouse embryos from E11.5 to P1. Fluorescence images of cardiomyocytes expressing Fucci green, Fucci red, and cells immunostained for Nkx2.5 in trabecular layer (Tb) and compact layer (Co). Scale bars, 100 μm. B. The percentages of S/G2/M phase cardiomyocytes in the compact layer and trabecular layer from E11.5 to P1 ($n = 3$–5). ** $P < 0.01$; NS, no significant difference.

G2/M phase cardiomyocyte population peaked at E11.5 and diminished with development (Fig. 2B and C). Previous reports that the cardiomyocyte cell cycle stopped near the term, could be interrogated further in this study. We did not see a significant difference in cell cycle dynamics between the left and right atrium or within the ventricle (Fig. 2B and C).

Developing hearts have regional differences in cardiomyocyte populations with respect to cell cycle dynamics, such as in the compact layer versus the trabecular layer [20,21]. As expected, cardiomyocytes in the compact layer showed a larger S/G2/M phase population than the trabecular layer during early developing stages (Fig. 3A and B). This anatomical difference gradually diminished during development. In addition, the outflow tract region showed a significantly low population of the S/G2/M phase cardiomyocytes compared to the ventricles in Fucci-green-expressing E10 transgenic mice (Fig. S2A, B, C). These findings agree with prior studies which report low proliferative capacity in the trabecular layer and outflow tract [22,23].

3.4. Establishing a cardiac ex vivo culture method

For live imaging, we planned to establish a cardiac ex vivo culture method. E11.5 mouse embryos were anesthetized by induced hypothermia, and hearts were quickly extracted and then placed, either whole or sliced, in an agarose gel. Following re-warming in an incubator, the extracted heart tissue started beating spontaneously. EdU, a nucleoside analog to thymidine, is incorporated into newly synthesized DNA and often used to evaluate cell cycle progression [24]. We therefore used EdU labeling as a reliable and standardized method to evaluate and compare the cell cycle progression of in vivo and ex vivo cultured cardiomyocytes. Fucci-green-expressing pregnant mice at 11.5 days post coitum (dpc) were intraperitoneally (i.p.) injected with 200 μg EdU. Embryo hearts were analyzed with immunofluorescence staining for Nkx2.5 and EdU. As expected, EdU-incorporated cardiomyocytes also showed Fucci-green expression (Fig. S3A). Representative non-cardiomyocyte populations such as endothelial cells (CD31), hematopoietic cells (CD45), fibroblasts (collagen type 1), and smooth muscle cells (calponin) showed no visible Fucci-green expression in heart, regardless of EdU incorporation (Fig. S3B). This re-confirmed the distinct strength of Fucci fluorescence of cardiomyocytes.

To assess in vivo cardiomyocyte cell cycle progression, 11.5 dpc wild-type mice were i.p. injected with 200 μg EdU. Two hours after the injection, in vivo EdU labeled embryo heart ventricles were immunostained for Nkx2.5 and EdU (Fig. 4A), and up to 20.5% ± 1.2% of cardiomyocytes were labeled with EdU in vivo (Fig. 4D). To assess cell cycle progression in ex vivo cultured cardiomyocyte, whole or sliced wild-type E10.5 heart was incubated in culture medium. EdU labeling was performed for 2 h in 1 mM EdU-containing medium, starting at 24 h after placing in control culture medium, to determine the effect of culture on ventricular cardiomyocyte proliferation. After a total of 26 h of incubation, Nkx2.5 and EdU were visualized by immunofluorescence staining in whole (Fig. 4B) or sliced (Fig. 4C) wild-type E10.5 heart ventricles.

Different concentrations of oxygen and serum (fetal bovine serum; FBS) were tested in E10.5 ex vivo-cultured samples to determine the optimum condition. We tested five different oxygen concentrations (0.1%, 1%, 5%, 20%, 40%) with standard FBS concentration (10%). There were no cells alive after 26 h of culture in severe hypoxic (0.1%) condition (data not shown). Both whole and sliced heart cultured ex vivo showed a significant decrease in EdU-positive cardiomyocyte population under low oxygen concentration, compared to room air and high oxygen concentration (Fig. 4E). FBS was also tested in four different conditions (0.1%, 10%, 20%, 95%) with standard oxygen concentration (20%). EdU-positive cardiomyocytes showed no significant difference between different FBS concentrations, in whole and

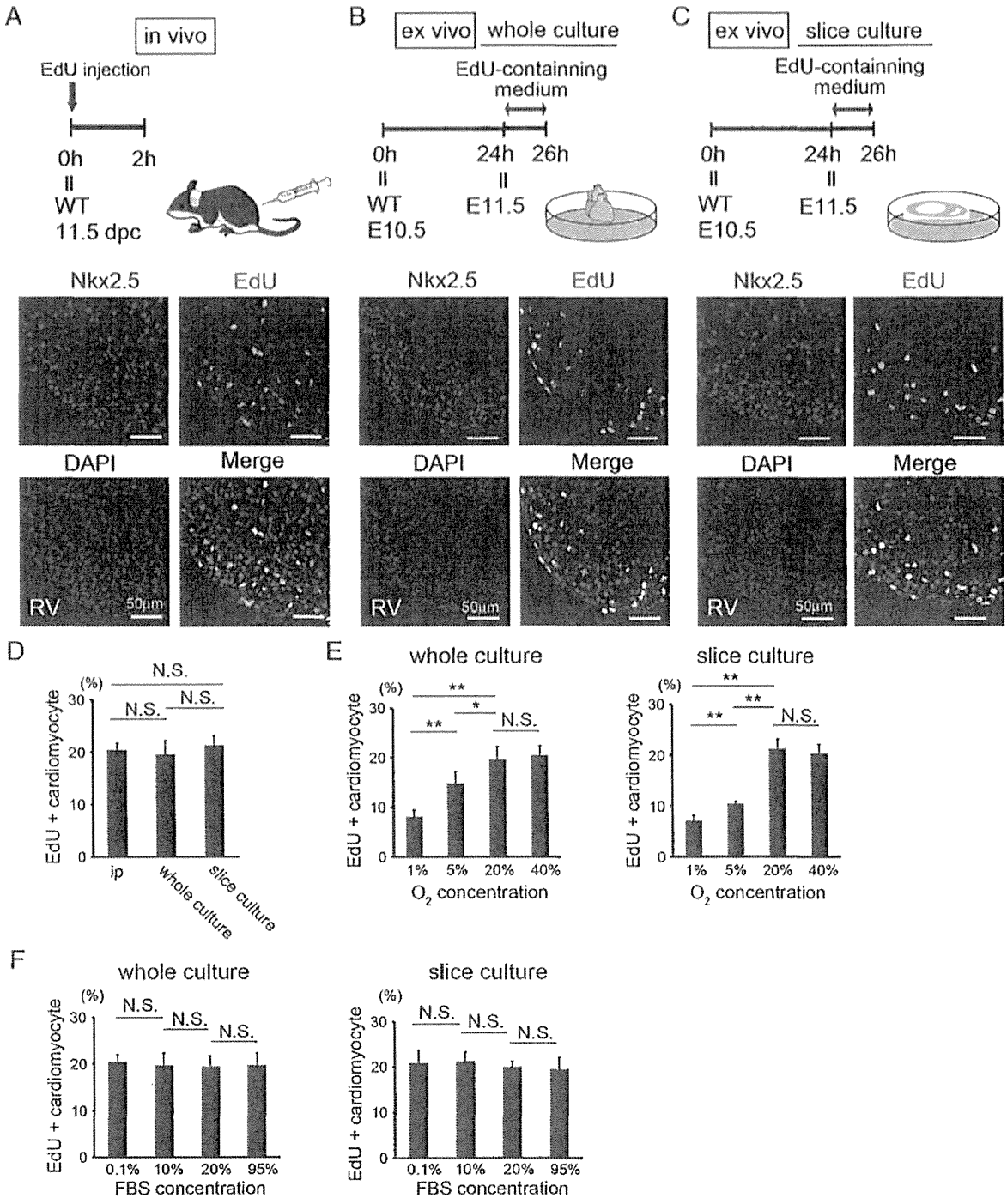

Fig. 4. Consideration of oxygen and serum concentration for cardiac ex vivo culture method. A. EdU labeling method for in vivo cardiomyocyte cell cycle analysis. Wild type mouse embryos at E11.5 were labeled with EdU as described in scheme. Immunofluorescence images of cells immunostained for Nkx2.5, DAPI, and EdU in right ventricles are shown in the sections. Scale bars, 50 μm. B and C. EdU labeling method for whole (B) and sliced (C) ex vivo cultured cardiomyocyte cell cycle analysis. Wild type mouse embryonic hearts at E11.5 were labeled with EdU as described in scheme. Immunofluorescence images of cells immunostained for Nkx2.5, DAPI, and EdU in right ventricles are shown in the sections of ex vivo cultured embryonic heart. Scale bars, 50 μm. D. The percentages of EdU positive cardiomyocytes in in vivo and whole or sliced ex vivo cultured heart at O_2 20% concentration and 10% FBS concentration ($n = 4$–8). E. The percentages of EdU positive cardiomyocytes at different O_2 concentrations in whole heart culture and cardiac slice culture ($n = 4$–8). F. The percentages of EdU positive cardiomyocytes at different FBS concentrations in whole heart culture and cardiac slice culture ($n = 4$–8). ** $P < 0.01$, * $P < 0.05$; NS, no significant difference.

slice ex vivo cultures (Fig. 4F). Based on these results, we decided on an optimal condition for cardiac ex vivo culture as oxygen concentration of 20% and FBS concentration of 10%. In this condition, there was no significant difference in the percentage of EdU-positive ventricular cardiomyocytes between in vivo, and ex vivo whole and slice culture (Fig. 4D).

3.5. Successful time-lapse imaging of cardiomyocytes during development

Finally we performed time-lapse imaging by combining the ex vivo culture method and the Fucci system. Cardiac slices were made from E11.5, E14.5, E18.5, and P1 Fucci-red/green-expressing transgenic mice (Fig. S4). Live imaging successfully visualized the cell cycle

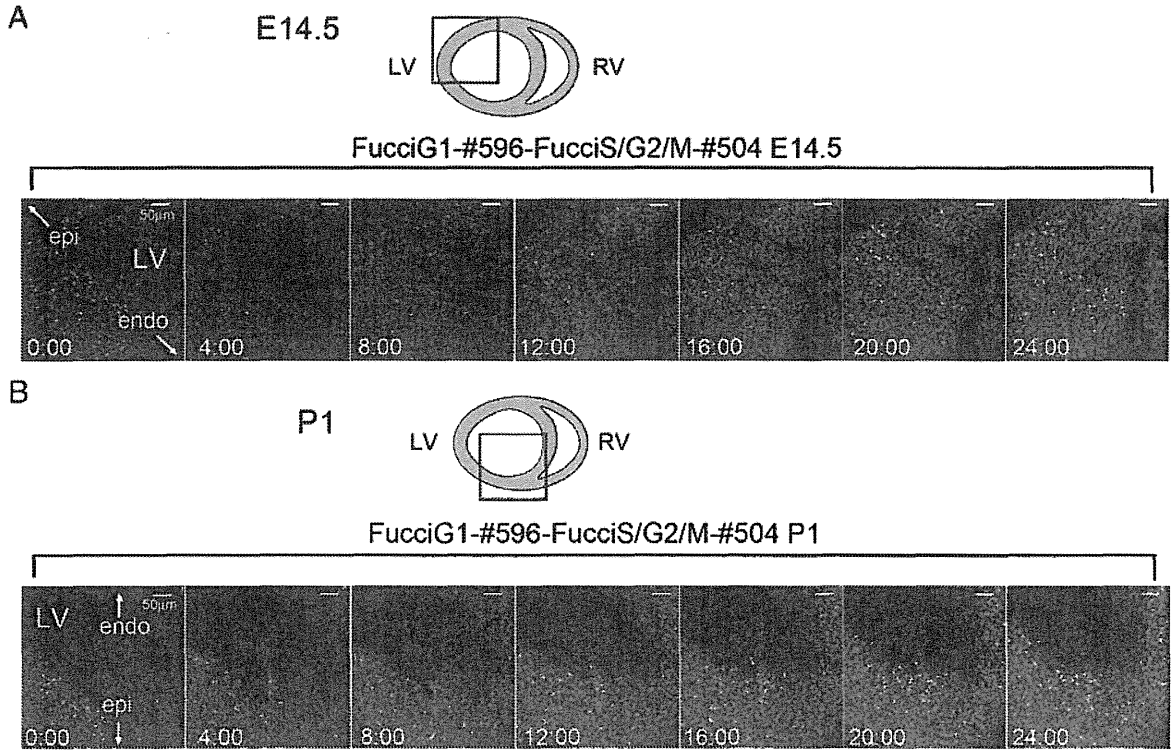

Fig. 5. Time-lapse imaging of ex vivo cultured cardiomyocytes. A. Time-dependent change of cardiomyocyte cell cycle progression in E14.5 left ventricle by applying the ex vivo culture method to the Fucci system (Fucci-expressing (#596/#504) transgenic mice). B. Time-dependent change of cardiomyocyte cell cycle progression in P1 left ventricle by applying the ex vivo culture method to the Fucci system (Fucci-expressing (#596/#504) transgenic mice). The cell cycle progression of cardiomyocytes is visualized, as fluorescent colors in the nuclei changed from red (G1) to yellow (G1/S), green (S/G2/M), and then green extinction (M). Scale bars, 50 μm.

progression of cardiomyocytes, as fluorescent colors in the nuclei changed from red to yellow and then green, suggesting the cell cycle transition from the G1 phase to S phase and then S/G2/M phase (Fig. 5A, B, Movies S1, S2).

3.6. Cell cycle length dynamics in developing heart

Using the Fucci system, we could also directly measure the length of an S/G2/M phase. Each phase was represented respectively by Fucci-green-positive nuclei and Fucci-green associated with dissolving nuclei, in living ex vivo cultured cardiomyocytes (Fig. 6A and B). The length of the S/G2/M phase, defined from the start of green fluorescence appearing to the completion of the nucleus division associated with green fluorescence disappearance, was measured at different developmental stages from E11.5, E14.5, E18.5, and P1 hearts. Interestingly, the S/G2/M phase length in cardiomyocytes elongated during development (E14.5; 10.4 h ± 1.2 h, P1; 15.2 h ± 1.2 h) (Fig. 6C). These data help us to understand the heart morphogenesis by calculating the cell proliferation. To reconfirm the difference of the S/G2/M phase length among different development stages, we used a combination of EdU labeling and Fucci expression. Fucci-green-expressing pregnant mice were i.p. injected with 200 μg EdU, and embryos were fixed at 2, 6, and 14 h after injection (Fig. S5A and B). Since EdU labels S phase at the injection point and Fucci-green visualizes the ongoing real time S/G2/M phase, the populations of both EdU+ and Fucci-green+ cardiomyocytes gradually decreased after injection (Fig. S5C). As expected, E18.5 embryos had a higher percentage of both EdU+ and Fucci-green+ cardiomyocytes compared to E11.5 embryos, which suggested a longer S/G2/M phase length in E18.5 hearts. We calculated the cardiomyocyte total cell cycle (T_C) length, by dividing the S/G2/M phase length with the ratio of the S/G2/M phase to growth fraction [25,26]. Growth fraction was counted by immunostaining each murine heart ventricle with Nkx2.5 and Ki67 antibody [27] (Fig. S6A and B). Estimated T_C length and G1 phase length resulted in the longest T_C length in E18.5 and the shortest G1 phase length in P1 (Fig. S6C and D). These data support that time-lapse imaging by using ex vivo culture and Fucci-expressing transgenic mouse reveals cardiomyocyte cell cycle dynamics during development in a visually comprehensive fashion.

4. Discussion

Our study presents an establishment of a cardiac ex vivo culture method, accompanied by observation of cardiomyocyte cell cycle dynamics by live imaging. Initially, we confirmed that Fucci probes represent cell cycle phase in murine cardiomyocytes. Fucci system uses the CAG promoter, and gene expression under the CAG promoter is not specific for cardiomyocyte, but observed in a broad spectrum of tissues in transgenic mice [28]. In this study, we observed only the heart of Fucci red/green-expressing transgenic mouse line. We found that preferential strong expression was detected in cardiomyocyte in the heart as described and this transgenic line was suitable for the experiment. PCNA is up regulated not only in S phase, but also during DNA repair, so we covered the shortcoming with PHH3 staining and EdU labeling [13,14,24,29]. Then we optimized the ex vivo culture condition to minimize the differences in EdU incorporation between in vivo and ex vivo cultured cardiomyocyte. Our cardiac ex vivo culture condition was aimed to improve the previous methods that basically examined cardiac tissue in whole embryo culture.

Oxygen concentrations range from 1% to 5% in the uterine environment, and effects of different oxygen concentrations on the development of rodent embryo culture have been discussed in the past few

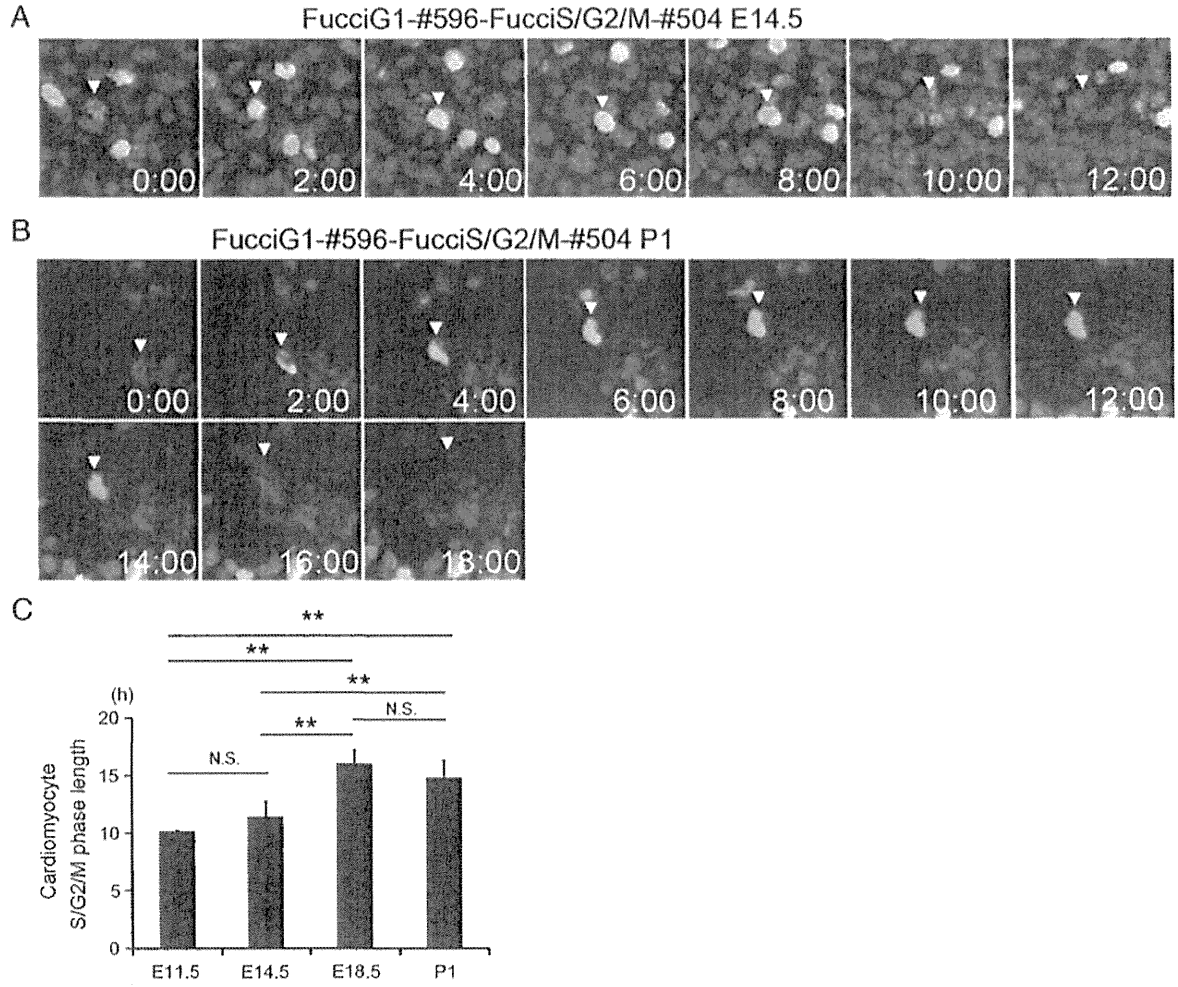

Fig. 6. Cardiomyocyte S/G2/M phase length measured by time-lapse imaging of Fucci transgenic mouse. A and B. Representative individual cardiomyocyte nucleus showing the length of S/G2/M phase in time-lapse imaging of E14.5 (A) and P1 (B). C. The length of S/G2/M phase represented by Fucci green positive nuclei in living cardiomyocytes at different developmental stages from E11.5, E14.5, E18.5 and P1 (n = 4–8, 8–12 cardiomyocytes counted per each sample). * $P < 0.05$, ** $P < 0.01$; NS, no significant difference.

decades [30–33]. Optimal oxygen concentration for embryonic development differs in developmental stages, where early stage embryos (~E9.5) tend to favor hypoxic conditions compared to later stages. Oxygen concentration also strongly influences development of the heart [34–36]. The myocardium is broadly hypoxic at E9.5, but by E13.5, hypoxia is restricted to the myocardium of the outflow tract, interventricular septum, and atrioventricular cushions [36–38]. However, ex vivo culture provides a different environment compared to in vivo. For example, lack of extracardiac signals and mechanical stress may influence cytoskeletal organization and gene expression in ex vivo culture cardiomyocytes [39–41]. Important modulators of the development and expansion of cardiac chambers such as closed functional embryonic circulation and coronary blood flow, are lost in ex vivo condition which are established around E10–E12 and E14–E16, respectively [35,42–44]. Loss of hemoglobin (red blood cell) also affects difference in environment such as oxygen supply [35]. Thus, it is important to understand that ex vivo cultured heart still exists in different circumstances.

No prior study has successfully examined cell cycle length directly in cardiomyocytes, mainly due to the lack of methods to directly measure this parameter. A traditional method is to measure the population doubling time and then calculate each cell cycle phase from the ratio of their cell cycle marker expression [25]. However, this method is not accurate because it only works on the premise that every cell continuously enters the cell cycle and has the same length of cell cycle phases such as cancer cells [45]. By combining Fucci system with our ex vivo culture method, we revealed that the cardiomyocyte S/G2/M phase prolongs during development. It is ideal to measure the full cell cycle length including the G1 phase; however, it was often difficult to follow a single cardiomyocyte since the Fucci fluorescence disappears immediately after the M phase, and most of the cells that finished their M phase during observation already showed a red signal from the beginning. This could mean that the total cardiomyocyte cell cycle length is longer than 24 h, which was the limit of our current live imaging. The estimated total cell cycle length of ventricular cardiomyocyte calculated by the ratio of the S/G2/M phase to growth fraction, was around 30–35 h, exceeding 24 h.

It is important to reveal cell cycle dynamics in cardiomyocytes, particularly with respect to the need to control cardiomyocyte proliferation and develop adult cardiac regenerative therapy. Cell cycle length of the heart has been estimated mainly by methods utilizing DNA synthesis analysis, targeted in various cell types and species [23,46–50]. Results in total cell cycle length vary between several hours and several days, according to targeted regions, developmental stages, cell types, and species. Our estimated total cell cycle length in ventricular cardiomyocyte consists of prior reports and we revealed elongation of the cardiomyocyte cell cycle phase during development, but the difference between in vivo and our ex vivo study should be noticed.

This study established a novel cardiac ex vivo culture method for live imaging in murine heart. As a consequence, we found a gradual elongation of the S/G2/M phase length during development in living cardiomyocytes.

Supplementary data to this article can be found online at http://dx.doi.org/10.1016/j.yjmcc.2014.03.020.

Non-standard abbreviations and acronyms

cTnT	cardiac troponin T
EdU	5-ethynyl-20-deoxyuridine
Fucci	fluorescent ubiquitination-based cell cycle indicator
FACS	fluorescence-activated cell sorter
FBS	fetal bovine serum
PBS	phosphate-buffered saline
PCNA	proliferating cell nuclear antigen
PHH3	phosphohistone H3
TBS	Tris-buffered saline
dpc	days post coitum

Sources of funding

This study was supported in part by research grants from the Ministry of Education, Culture, Sports, Science and Technology, Japan, by the Graduate School Doctoral Student Aid Program, Keio University, Japan, by the Heart Foundation Young Investigator's Research Grant, and by the Keio University Grant-in-Aid for Encouragement of Young Medical Scientists.

Disclosures

None.

Acknowledgments

We thank Y. Shimizu and Y. Miyake for technical assistance.

References

[1] Soonpaa MH, Kim KK, Pajak L, Franklin M, Field LJ. Cardiomyocyte DNA synthesis and binucleation during murine development. Am J Physiol 1996;271:H2183–9.
[2] Anversa P, Nadal-Ginard B. Myocyte renewal and ventricular remodelling. Nature 2002;415:240–3.
[3] Yuasa S, Fukuda K, Tomita Y, Fujita J, Ieda M, Tahara S, et al. Cardiomyocytes undergo cells division following myocardial infarction is a spatially and temporally restricted event in rats. Mol Cell Biochem 2004;259:177–81.
[4] Porrello ER, Mahmoud AI, Simpson E, Hill JA, Richardson JA, Olson EN, et al. Transient regenerative potential of the neonatal mouse heart. Science 2011;331:1078–80.
[5] Soonpaa MH, Field LJ. Survey of studies examining mammalian cardiomyocyte DNA synthesis. Circ Res 1998;83:15–26.
[6] Laflamme MA, Murry CE. Heart regeneration. Nature 2011;473:326–35.
[7] de la Pompa JL, Epstein JA. Coordinating tissue interactions: Notch signaling in cardiac development and disease. Dev Cell 2012;22:244–54.
[8] Miyata T, Kawaguchi A, Okano H, Ogawa M. Asymmetric inheritance of radial glial fibers by cortical neurons. Neuron 2001;31:727–41.
[9] Tabata H, Nakajima K. Multipolar migration: the third mode of radial neuronal migration in the developing cerebral cortex. J Neurosci 2003;23:9996–10001.
[10] Sakaue-Sawano A, Kurokawa H, Morimura T, Hanyu A, Hama H, Osawa H, et al. Visualizing spatiotemporal dynamics of multicellular cell-cycle progression. Cell 2008;132:487–98.
[11] Vodermaier HC. APC/C and SCF: controlling each other and the cell cycle. Curr Biol 2004;14:R787–96.
[12] Nishitani H, Lygerou Z, Nishimoto T, Nurse P. The Cdt1 protein is required to license DNA for replication in fission yeast. Nature 2000;404:625–8.
[13] Bravo R, Macdonald-Bravo H. Existence of two populations of cyclin/proliferating cell nuclear antigen during the cell cycle: association with DNA replication sites. J Cell Biol 1987;105:1549–54.
[14] Goto H, Tomono Y, Ajiro K, Kosako H, Fujita M, Sakurai M, et al. Identification of a novel phosphorylation site on histone H3 coupled with mitotic chromosome condensation. J Biol Chem 1999;274:25543–9.
[15] Okabe M, Ikawa M, Kominami K, Nakanishi T, Nishimune Y. 'Green mice' as a source of ubiquitous green cells. FEBS Lett 1997;407:313–9.
[16] Alexopoulou AN, Couchman JR, Whiteford JR. The CMV early enhancer/chicken beta actin (CAG) promoter can be used to drive transgene expression during the differentiation of murine embryonic stem cells into vascular progenitors. BMC Cell Biol 2008;9:2.
[17] Baudino TA, Carver W, Giles W, Borg TK. Cardiac fibroblasts: friend or foe? Am J Physiol Heart Circ Physiol 2006;291:H1015–26.
[18] Walsh S, Ponten A, Fleischmann BK, Jovinge S. Cardiomyocyte cell cycle control and growth estimation in vivo—an analysis based on cardiomyocyte nuclei. Cardiovasc Res 2010;86:365–73.
[19] Banerjee I, Fuseler JW, Price RL, Borg TK, Baudino TA. Determination of cell types and numbers during cardiac development in the neonatal and adult rat and mouse. Am J Physiol Heart Circ Physiol 2007;293:H1883–91.
[20] Ben-Shachar G, Arcilla RA, Lucas RV, Manasek FJ. Ventricular trabeculations in the chick embryo heart and their contribution to ventricular and muscular septal development. Circ Res 1985;57:759–66.
[21] Sedmera D, Pexieder T, Vuillemin M, Thompson RP, Anderson RH. Developmental patterning of the myocardium. Anat Rec 2000;258:319–37.
[22] Toyoda M, Shirato H, Nakajima K, Kojima M, Takahashi M, Kubota M, et al. Jumonji downregulates cardiac cell proliferation by repressing cyclin D1 expression. Dev Cell 2003;5:85–97.
[23] Sedmera D, Reckova M, DeAlmeida A, Coppen SR, Kubalak SW, Gourdie RG, et al. Spatiotemporal pattern of commitment to slowed proliferation in the embryonic mouse heart indicates progressive differentiation of the cardiac conduction system. Anat Rec A Discov Mol Cell Evol Biol 2003;274:773–7.
[24] Salic A, Mitchison TJ. A chemical method for fast and sensitive detection of DNA synthesis in vivo. Proc Natl Acad Sci U S A 2008;105:2415–20.
[25] Nowakowski RS, Lewin SB, Miller MW. Bromodeoxyuridine immunohistochemical determination of the lengths of the cell cycle and the DNA-synthetic phase for an anatomically defined population. J Neurocytol 1989;18:311–8.
[26] Arai Y, Pulvers JN, Haffner C, Schilling B, Nusslein I, Calegari F, et al. Neural stem and progenitor cells shorten S-phase on commitment to neuron production. Nat Commun 2011;2:154.
[27] Scholzen T, Gerdes J. The Ki-67 protein: from the known and the unknown. J Cell Physiol 2000;182:311–22.
[28] Hayashi S, McMahon AP. Efficient recombination in diverse tissues by a tamoxifen-inducible form of Cre: a tool for temporally regulated gene activation/inactivation in the mouse. Dev Biol 2002;244:305–18.
[29] Essers J, Theil AF, Baldeyron C, van Cappellen WA, Houtsmuller AB, Kanaar R, et al. Nuclear dynamics of PCNA in DNA replication and repair. Mol Cell Biol 2005;25:9350–9.
[30] Okazaki K, Maltepe E. Oxygen, epigenetics and stem cell fate. Regen Med 2006;1:71–83.
[31] Miyata T, Kawaguchi A, Saito K, Kuramochi H, Ogawa M. Visualization of cell cycling by an improvement in slice culture methods. J Neurosci Res 2002;69:861–8.
[32] New DA, Coppola PT. Effects of different oxygen concentrations on the development of rat embryos in culture. J Reprod Fertil 1970;21:109–18.
[33] Miki A, Fujimoto E, Ohsaki T, Mizoguti H. Effects of oxygen concentration on embryonic development in rats: a light and electron microscopic study using whole-embryo culture techniques. Anat Embryol 1988;178:337–43.
[34] Dunwoodie SL. The role of hypoxia in development of the mammalian embryo. Dev Cell 2009;17:755–73.
[35] Fisher SA, Burggren WW. Role of hypoxia in the evolution and development of the cardiovascular system. Antioxid Redox Signal 2007;9:1339–52.
[36] Liu H, Fisher SA. Hypoxia-inducible transcription factor-1alpha triggers an autocrine survival pathway during embryonic cardiac outflow tract remodeling. Circ Res 2008;102:1331–9.
[37] Ream M, Ray AM, Chandra R, Chikaraishi DM. Early fetal hypoxia leads to growth restriction and myocardial thinning. Am J Physiol Regul Integr Comp Physiol 2008;295:R583–95.
[38] Sugishita Y, Watanabe M, Fisher SA. Role of myocardial hypoxia in the remodeling of the embryonic avian cardiac outflow tract. Dev Biol 2004;267:294–308.
[39] Manner J, Seidl W, Steding G. The role of extracardiac factors in normal and abnormal development of the chick embryo heart: cranial flexure and ventral thoracic wall. Anat Embryol 1995;191:61–72.
[40] Auman HJ, Coleman H, Riley HE, Olale F, Tsai HJ, Yelon D. Functional modulation of cardiac form through regionally confined cell shape changes. PLoS Biol 2007;5:e53.
[41] Yamazaki T, Komuro I, Nagai R, Yazaki Y. Stretching the evidence in the case of cardiac growth. Cardiovasc Res 1996;31:493–8.
[42] Zak R, Kizu A, Bugaisky L. Cardiac hypertrophy: its characteristics as a growth process. Am J Cardiol 1979;44:941–6.
[43] Hove JR, Koster RW, Forouhar AS, Acevedo-Bolton G, Fraser SE, Gharib M. Intracardiac fluid forces are an essential epigenetic factor for embryonic cardiogenesis. Nature 2003;421:172–7.
[44] Xu B, Doughman Y, Turakhia M, Jiang W, Landsettle CE, Agani FH, et al. Partial rescue of defects in Cited2-deficient embryos by HIF-1alpha heterozygosity. Dev Biol 2007;301:130–40.
[45] Salomoni P, Calegari F. Cell cycle control of mammalian neural stem cells: putting a speed limit on G1. Trends Cell Biol 2010;20:233–43.
[46] Sedmera D, Thompson RP. Myocyte proliferation in the developing heart. Dev Dyn 2011;240:1322–34.
[47] Mikawa T, Borisov A, Brown AM, Fischman DA. Clonal analysis of cardiac morphogenesis in the chicken embryo using a replication-defective retrovirus: I. Formation of the ventricular myocardium. Dev Dyn 1992;193:11–23.

[48] van den Berg G, Abu-Issa R, de Boer BA, Hutson MR, de Boer PA, Soufan AT, et al. A caudal proliferating growth center contributes to both poles of the forming heart tube. Circ Res 2009;104:179–88.
[49] de Boer BA, van den Berg G, Soufan AT, de Boer PA, Hagoort J, van den Hoff MJ, et al. Measurement and 3D-visualization of cell-cycle length using double labelling with two thymidine analogues applied in early heart development. PLoS One 2012;7: e47719.
[50] Ferreira-Martins J, Ogorek B, Cappetta D, Matsuda A, Signore S, D'Amario D, et al. Cardiomyogenesis in the developing heart is regulated by c-kit-positive cardiac stem cells. Circ Res 2012;110:701–15.